

A Hybrid Method for Efficient and Accurate Simulations of Diffusion Compartment Imaging Signals

Gaëtan Rensonnet^a, Damien Jacobs^a, Benoît Macq^a and Maxime Taquet^{a,b}

^aICTEAM Institute, Université catholique de Louvain, Louvain-la-Neuve, Belgium;

^bComputational Radiology Laboratory, Boston Children’s Hospital, Harvard Medical School, Boston, MA, USA.

ABSTRACT

Diffusion-weighted imaging is sensitive to the movement of water molecules through the tissue microstructure and can therefore be used to gain insight into the tissue cellular architecture. While the diffusion signal arising from simple geometrical microstructure is known analytically, it remains unclear what diffusion signal arises from complex microstructural configurations. Such knowledge is important to design optimal acquisition sequences, to understand the limitations of diffusion-weighted imaging and to validate novel models of the brain microstructure. We present a novel framework for the efficient simulation of high-quality DW-MRI signals based on the hybrid combination of exact analytic expressions in simple geometric compartments such as cylinders and spheres and Monte Carlo simulations in more complex geometries. We validate our approach on synthetic arrangements of parallel cylinders representing the geometry of white matter fascicles, by comparing it to complete, all-out Monte Carlo simulations commonly used in the literature. For typical configurations, equal levels of accuracy are obtained with our hybrid method in less than one fifth of the computational time required for Monte Carlo simulations.

Keywords: Diffusion-weighted MRI, Monte Carlo simulation, Multiple-correlation function, Dictionary

1. INTRODUCTION

Diffusion-weighted magnetic resonance imaging (DW-MRI) is a non-invasive, in vivo imaging modality sensitive to the motion of water molecules through the tissues in the direction of an externally-applied magnetic gradient. Since tissues act as barriers to the free diffusion of water molecules, DW-MRI measurements are used to infer information on their microscopic spatial configuration, a discipline known as *microstructure imaging*. In a brain voxel, microstructural parameters of interest include the number and orientation of fascicles of axons, the axons’ mean diameter and the axonal density.

We identify three reasons motivating the study of the efficient simulation of high-accuracy DW-MRI data. First, synthetic data is often used as ground-truth information to validate parametric models expressing DW-MRI signals as a function of the underlying microstructure and of the applied magnetic gradient. Second, knowing the diffusion signal arising from complex microstructural geometries would help determine the optimal acquisition sequence to measure microstructural properties of interest.¹ Third, we believe that quantitative microstructure estimation based on large collections or dictionaries of pre-computed DW-MRI signals could play an important role in the future. Research in that direction has been undertaken in Ref. 2 for instance, with pre-computed signals based on a very simple physical model. Considering more accurate, physically realistic DW-MRI signals could lead to better quantitative microstructure estimation.

We therefore consider physically-relevant models of brain microstructure based on water compartments (typically shaped like cylinders and spheres to model the brain’s axons and glial cells) rather than phenomenological models based on simplified analytical expressions of the diffusion signal, such as multi-tensor models,³ NODDI,⁴ CHARMED⁵ or DIAMOND.⁶ The geometric regularity of these shapes can be exploited by an efficient analytic

Further author information: (Send correspondence to G.R.)

G.R.: E-mail: gaetan.rensonnet@student.uclouvain.be,

M.T.: E-mail: Maxime.Taquet@childrens.harvard.edu,

B.M.:E-mail: benoit.macq@uclouvain.be.

tool known as the multiple correlation function (MCF) approach.⁷ The signal contribution due to water outside these regularly-shaped compartments, referred to as the *extra-cellular* signal, will be dealt with numerically using Monte Carlo (MC) simulations, more computationally intensive but able to provide arbitrary precision if the statistical sampling is sufficiently large.

Section 2 describes the analytic method and the numerical method we selected and how they are combined through a convenient superposition principle that holds under the slow-exchange hypothesis, which we recall below. This hybrid method is then validated in Sec. 3 on three simple microstructural configurations based on cylindrical water compartments by comparing our results to complete MC simulations making no use of analytic results, generally considered to provide ground-truth.^{8,9}

2. HYBRID METHOD : THEORY

We focus on the widely-used PGSE sequence characterized by a gradient direction $\hat{\mathbf{g}}$, gradient intensity G , gradient duration δ and diffusion time Δ . The problem is to find the value of the DW-MRI signal $E_{pgse}(\Omega)$ associated with the diffusion environment or microstructure configuration Ω , which is obtained through the resolution of the Bloch-Torrey PDE in Ω .¹⁰ Sections 2.2 and 2.3 describe, respectively, the analytic and the numerical method we have selected to solve that PDE and obtain relevant PGSE signals in specific types of compartments. The slow-exchange hypothesis, recalled below in Sec. 2.1, enables effective combination of the signals obtained by either method in an accurate and efficient hybrid simulation procedure, which we describe in Sec. 2.4.

2.1 Slow-exchange hypothesis

If the diffusion environment Ω can be expressed as the union of K mutually-disjoint compartments $\Omega_1, \dots, \Omega_K$ with volumes $|\Omega_1|, \dots, |\Omega_K|$ and with perfectly-reflecting boundaries, then the total signal $E_{pgse}(\Omega)$ in the diffusion environment Ω is obtained as

$$E_{pgse}(\Omega) = \sum_{i=1}^K f_i E_{pgse}(\Omega_i), \quad (1)$$

where $f_i = \frac{|\Omega_i|}{|\Omega|}$ and $E_{pgse}(\Omega_i)$, for $i = 1, \dots, K$, are respectively the volume fractions and the individual signal contributions of each compartment. This result holds if the T2 characteristic time and the proton density is uniform across all subdomains Ω_i .

In practice, cell membranes are seldom completely impermeable. However, at the time scale of a DW-MRI acquisition, typically of the order of 100 ms, we may consider that little molecule transfer between compartments occurs.^{9,11} This is referred to as the *slow-exchange limit*.

2.2 Multiple correlation function approach

Grebenkov's multiple correlation function approach⁷ is a unified mathematical framework for solving the Bloch-Torrey PDE based on the decomposition of the solution into Laplace eigenfunctions. It yields *exact* results for a sequence of applied magnetic gradients with fixed direction and piecewise-constant intensity profile such as encountered in a PGSE acquisition.

If we consider a microstructural environment Ω of typical length scale L_0 (for instance, Ω could be an infinitely-long cylinder and L_0 its radius), the DW-MRI signal $E_{MCF,pgse}(\Omega)$ associated to the PGSE parameters $\hat{\mathbf{g}}, G, \Delta, \delta$ is *exactly* given by

$$E_{MCF,pgse}(\Omega) = \left[\underbrace{e^{-(p\Lambda - iq\mathcal{B})\frac{\delta}{T}}}_{\text{gradient rephasing}} \underbrace{e^{-p\Lambda\frac{(\Delta-\delta)}{T}}}_{\text{pure diffusion}} \underbrace{e^{-(p\Lambda + iq\mathcal{B})\frac{\delta}{T}}}_{\text{gradient dephasing}} \right]_{0,0}, \quad (2)$$

where $p = \frac{DT}{L_0^2}$ and $q = \gamma GL_0 T$ are two dimensionless numbers with D the diffusivity of the medium and T being related to the typical time scale of the PGSE experiment, for instance $T = \Delta + \delta$, where the exponentials are

matrix exponentials on the diagonal matrix Λ and the symmetric matrix \mathcal{B} , both of infinite dimension and where $[\cdot]_{0,0}$ denotes the first diagonal element. The matrices Λ and \mathcal{B} only depend on the geometry Ω through the resolution of the (time-independent) Laplace eigenvalue problem in Ω , which is simpler than directly solving the Bloch-Torrey PDE. They must be computed once and for all and can then be used for any PGSE parameters.

In practice, we will only keep the first M terms of the eigenfunction expansion, i.e. the first M lines and columns of Λ and \mathcal{B} , with M chosen so that

$$p\lambda_M \gg q, \quad (3)$$

where λ_i is the i -th diagonal element of Λ , thus ensuring that the real, damping factor $p\lambda$ dominates the imaginary, oscillating factor $iq\mathcal{B}$ in Eq. (2). This is justified by the strictly monotonous increase of the diagonal elements of Λ .¹² Note that Eq. (2) can not be further simplified since the matrices Λ and \mathcal{B} do not commute in general.

The MCF approach thus yields arbitrarily accurate DW-MRI signals for spatial domains or compartments in which the time-independent Laplace eigenvalue PDE can be solved, which includes spheres, disks (useful for infinitely-long cylinders) and finite-length cylinders. Evaluation of Eq. 2 is a matter of milliseconds on commonly available software such as MATLAB.

2.3 Monte Carlo simulations

A Monte Carlo simulation can be seen as a stochastic resolution of the Bloch-Torrey PDE from the microscopic level. The method chiefly consists in generating the diffusion trajectories of a number N of water molecules, also referred to as *spins* or *random walkers*. The phase ϕ of each spin due to its motion during the application of magnetic gradients is computed by integrating the resulting magnetic field over time numerically with some quadrature rule. This gives the normalized DW-MRI signal associated with each individual spin, $e^{i\phi}$. The DW-MRI signal is then calculated as the sample mean of the individual contributions.

More specifically, in an implementation such as the Camino Diffusion MRI Toolkit,^{13,14} the duration of the PGSE sequence is partitioned as $0 = t_0, t_1, \dots, t_T$ comprising T time increments of fixed duration δ_t . The accumulated phase ϕ of each spin is calculated using a rectangle quadrature rule, i.e. at every iteration $i = 0, \dots, T - 1$,

$$\phi(t_{i+1}) = \phi(t_i) + \gamma f(t_i) G \hat{\mathbf{g}} \cdot \mathbf{r}(t_i) \delta_t, \quad (4)$$

where γ is the gyromagnetic ratio of protons, $f(t)$ is the normalized temporal profile of the applied gradient, namely 1, 0 and -1 in a PGSE sequence, and $\mathbf{r}(t)$ is the simulated random trajectory of a given spin, made of discrete jumps of randomly chosen direction and of fixed step length L_{step} taken as

$$L_{step} = \sqrt{2nD\delta_t}, \quad (5)$$

where n is the spatial dimension of the diffusion environment Ω (e.g. $n = 2$ for the 2D-disk) and D is the diffusivity of the medium in Ω . The final normalized DW-MRI signal $E_{MC,pgse}(\Omega)$ is computed as the sample mean of $e^{i\phi}$

$$E_{MC,pgse}(\Omega) = \frac{1}{N} \sum_{k=1}^N e^{i\phi_k}. \quad (6)$$

Monte Carlo simulations thus allow to compute DW-MRI signals in any geometry Ω with an accuracy that increases arbitrarily in the limit $\delta_t \rightarrow 0$ and $N \rightarrow +\infty$. However, the computational burden is much heavier than for the analytic results presented in Sec. 2.2 for instance, especially for diffusion environments Ω of small typical length scale, for long PGSE sequences or for a high gradient intensity G . In practice, we will thus mostly resort to MC simulations to compute the signal associated to water molecules in the extra-cellular space, as the geometry of this environment is generally too complex to use more efficient analytic results.

2.4 Hybrid formula

Assuming that the diffusion environment or microstructure configuration Ω is made of mutually-disjoint compartments $\Omega_1, \dots, \Omega_K$ of respective volume fractions f_1, \dots, f_K , that the analytic MCF approach is applicable in the first K_a compartments and that there is little to no water exchange between the compartments, we can apply the superposition principle presented in Sec. 2.1 and obtain our total hybrid signal $E_{hyb}(\Omega)$ as

$$E_{hyb}(\Omega) = \sum_{i=1}^{K_a} f_i E_{MCF}(\Omega_i) + \sum_{i=K_a+1}^K f_i E_{MC}(\Omega_i), \quad (7)$$

where the PGSE subscripts have been omitted for clarity and where $E_{MCF}(\Omega_i)$ and $E_{MC}(\Omega_i)$ respectively represent the signals obtained by the analytic MCF and numerical MC methods.

3. HYBRID METHOD : VALIDATION

We validate the method presented in Sec. 2 on three types of microstructure configurations based on simple arrangements of cylinders described in Sec. 3.1. Section 3.2 briefly discusses the choice of parameters for the MCF method and most importantly for the MC simulations involved in the hybrid signal simulation method. We compare our results to complete MC simulations, considered to provide ground-truth data, in Sec. 3.3 and discuss the gain in efficiency-accuracy trade-off that our method offers compared to complete, traditional MC simulations in Sec. 3.4.

3.1 Synthetic phantoms of the microstructure

We consider the following brain microstructure configurations for the validation of the presented hybrid method.

- **Single fascicle of axons with identical radii** : Modeled by an infinite array of regularly-packed cylinders of infinite length and fixed radius r , placed a distance s from each other leading to a fraction f_{in} of *intra-axonal* space, i.e. the volume fraction occupied by the cylinders (see Fig. 1a). Here we choose $r = 3 \mu\text{m}$ and adjust s so that $f_{in} \approx 0.877$.
- **Single fascicle of axons with varying radii** : Modeled by 100 infinitely-long, parallel cylinders of varying radii packed in a square region of size l and periodically repeated to infinity (see Fig. 1b). The radii are drawn from a Gamma distribution $\Gamma(a, b)$, as suggested in Ref. 8 for its biological relevance. Here we select a shape parameter $a = 16.275$ and a scale parameter $b = 2.86 \times 10^{-6} \mu\text{m}$, corresponding to a distribution mean $\mu_r = ab = 0.465 \mu\text{m}$ and standard deviation $\sigma_r = \sqrt{ab} = 0.115 \mu\text{m}$. The 100 cylinders are packed into a square of side length $l = 10.45 \mu\text{m}$ through a trial-and-error algorithm implemented in Camino.¹³ The obtained radii lead to $f_{in} = 0.65$ and range from $r_{min} = 0.243 \mu\text{m}$ to $r_{max} = 1.025 \mu\text{m}$.
- **Crossing fascicles of axons with identical radii** : Modeled by two identical arrays of parallel cylinders characterized by the parameters r and f_{in} such as described above crossing in interleaved planes at an angle θ (see Fig. 2a). Here we set $\theta = \frac{\pi}{4}$, $r = 1 \mu\text{m}$ and adjust s so that $f_{in} \approx 0.71$.

In all three cases, the cylindrical compartments representing the axons of the brain are the water compartments wherein the analytic MCF method is applicable. The analytic formula (2) needs to be computed once in the first case (all cylinders are identical), 100 times in the second case and twice in the last case (one for each orientation). Note that for infinitely-long cylinders such as presented here, the diffusion is free and thus Gaussian along the axis of the cylinders and the MCF formula needs only be used for the components of the gradient that are perpendicular to the cylinders' axis.⁵

The extra-axonal water compartments present more complex geometric organization and will require a numerical MC simulation for each type of microstructure.

3.2 Selection of simulation parameters

Special care must be taken in selecting appropriate parameters both for the reference, ground-truth, complete MC simulations and for the hybrid signal simulations in order to obtain accurate results.

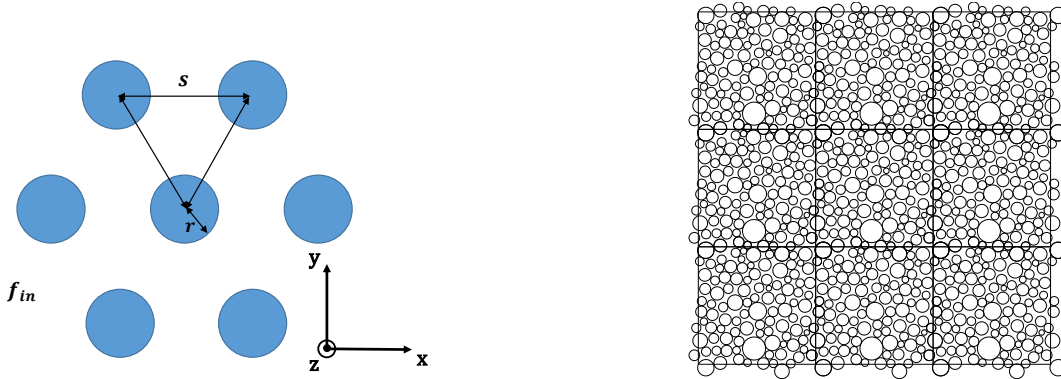
3.2.1 Parameters of the reference Monte Carlo simulations

As will be further discussed in Sec. 3.4, the statistical error of MC simulations typically decreases as $1/\sqrt{N}$ and a large enough N is therefore required. In the case of single fascicles with either fixed or varying radii, we select values of N_{MC} random walkers found in the literature through signal mean and variance analysis for similar microstructure configurations, as reported in Tab. 1. We slightly increase it for the crossing fascicle configuration to account for a less regular diffusion environment.

The number of time steps T determines the value of the time increments δ_t and of the fixed step length L_{step} defined in Eq. 5. Its value is therefore mainly impacted by the water compartments of smallest size, which is a major drawback of MC implementations with fixed step length. The value of δ_t should also be reduced (i.e. T increased) in the presence of magnetic gradients of high intensity G for the quadrature in Eq. 4 to remain relevant. We either took values found in the literature or computed it so as to make L_{step} comparable to the typical length scale of the diffusion environment.

3.2.2 Parameters of the hybrid signal simulations

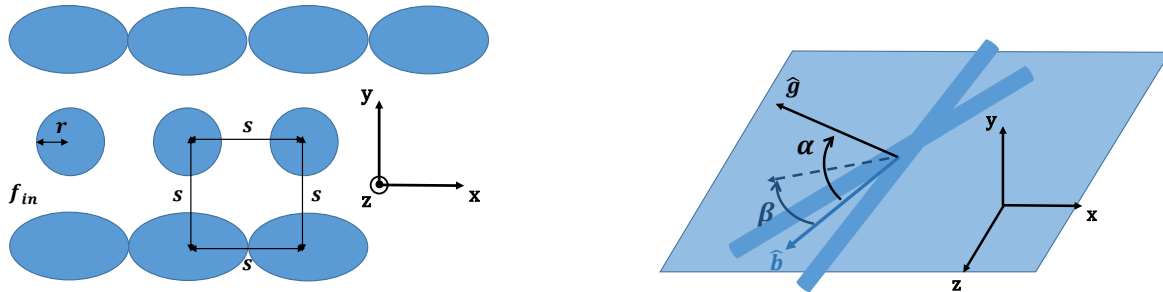
We set the truncation parameter of the MCF method to $M = 60$ in order to ensure nearly perfect signal accuracy in all three experiments, as discussed in Ref. 7.



(a) Hexagonal packing of cylinders of fixed radius r with cylinder separation s leading to an intra-axonal volume fraction f_{in} .

(b) Radius heterogeneity modeled by cylinders with radii drawn from a Gamma distribution and packed into a square region repeated to infinity.

Figure 1: **Single fascicles of axons modeled as regularly-packed parallel cylinders.** View in the xy -plane of two geometric models for single fascicles of axons based on cylinders of infinite length aligned with the z -axis.



(a) All cylinders have fixed radius r and the inter-cylinder separation s in each layer of cylinders leads to a given intra-axonal density f_{in} .

(b) All gradient directions $\hat{\mathbf{g}}$ are parametrized by the elevation angle α from the fascicles' plane, and the angle β between their projection into the fascicles' plane (dashed arrow) and the bisector $\hat{\mathbf{b}}$.

Figure 2: **Crossing fascicles modeled as arrays of axons crossing in interwoven planes.** One fascicle is directed along the z -axis and the second is rotated an angle α about the y -axis.

Since the random walkers are initially uniformly distributed across the diffusion environment, the MC simulation associated to the spins in the extra-axonal space required in the hybrid method could theoretically be run with a number $N_H \approx (1 - f_{in})N_{MC}$, if f_{in} represents the fraction of space inside the cylinders. We allow potentially better precision for the extra-axonal signal by taking slightly higher values of N_H , as reported in Tab. 1.

The value of T is left untouched since it is apparent in Figs. 1a, 1b and 2a that the diffusion areas of smallest length scale are located in the extra-axonal space, which is where the MC simulations are executed in the hybrid method.

Table 1: **Simulation parameters for the complete MC simulations and the extra-axonal MC simulations of the hybrid method.** Note that for the MC simulations of the hybrid method we can afford to take $N_H \geq (1 - f_{in})N_{MC}$, thus increasing quality, while maintaining $N_H \leq N_{MC}$, thus decreasing the simulation cost.

| Microstructure configuration | N_{MC} | N_H | $(1 - f_{in})N_{MC}$ | T |
|---------------------------------|-----------------------|--------|----------------------|--------------------|
| Single fascicle identical radii | 100 000 ¹⁴ | 20 000 | 12 300 | 1000 ¹⁴ |
| Single fascicle varying radii | 160 000 ⁸ | 62 000 | 56 000 | 5000 ⁸ |
| Crossing fascicles | 110 000 | 35 000 | 31 900 | 1200 |

3.3 Comparison to Complete Monte Carlo simulations

We choose to compute signals associated to PGSE parameters distributed over HARDI shells¹⁵ as these allow convenient representation of the obtained normalized signal $E(\Omega) = S/S_0$ (where S_0 is the detected signal in the absence of applied gradients). For the two single-fascicle configurations, the normalized signal can be plotted in 1D as a function of the dot product between the axis of the axons \mathbf{n} and the direction $\hat{\mathbf{g}} = \mathbf{g}/G$ of the applied gradient, as depicted in Figs. 3 and 4. In the case of crossing fascicles, a 2D representation is necessary in terms of the elevation angle α and the angle β from the fascicles' bisector, as illustrated in Figs. 2b and 5. All the HARDI shells used have 90 gradient directions and b-values indicated on the graphs.

It can be observed in Figs. 3, 4 and 5 that the results obtained with the hybrid method, in less computation time, is nearly impossible to distinguish from the traditional, all-out Monte Carlo simulations.

As expected, signal maxima seem to occur in directions where the diffusion as "seen by the gradient" is most restricted, i.e. when $\mathbf{n} \cdot \hat{\mathbf{g}} \approx 0$ in the case of single fascicles and in the direction normal to the crossing fascicles' plane, i.e. when $\alpha \approx 0$, in the third microstructural configuration. In the crossing fascicles' plane ($\alpha = 0$), maxima occur when the applied magnetic gradient is perpendicular to either one of the fascicles.

3.4 Precision-efficiency gain

We proceed to a simple variance analysis of the signal obtained by complete MC simulations and the hybrid signal presented above to analyze the gain in precision-efficiency trade-off offered by the use of analytic results along with MC simulations.

If we note $W_k = e^{i\phi_k}$ the random variable representing the (non-normalized) signal contribution of spin k , where ϕ_k is the accumulated phase shift, then the hybrid signal S_H is the random variable

$$S_H = f_{in}S_{in} + f_{ex}\frac{1}{N_H}\sum_{k=1}^N W_k,$$

where N_H is the number of spins used to simulate the extra-axonal signal and where S_{in} is the value obtained with the MCF method assumed applicable for the intra-axonal signal and considered deterministic and exact. The spins' trajectories (and any function thereof) are independent by definition, and we further assume that an initial uniform distribution of spins across the domain ensures that they are identically distributed, which allows to compute the variance σ_H^2 of S_H as a function of the variance σ_W^2 of all the random variables W_i

$$\sigma_H^2 = \frac{f_{ex}^2\sigma_W^2}{N_H}.$$

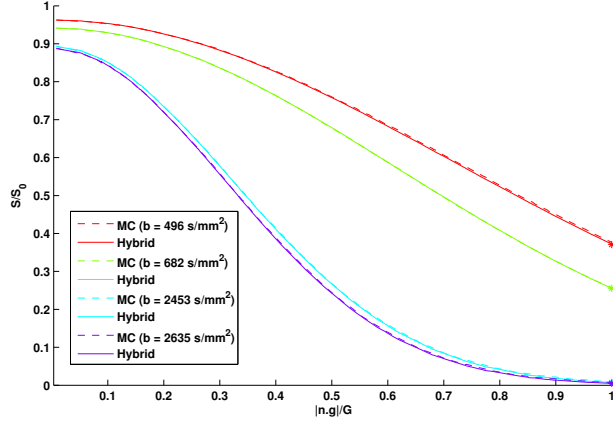


Figure 3: **Hybrid method yields ground-truth results for identical cylinders.** Total signal of an array of parallel cylinders obtained by complete MC simulations, considered exact, and by our hybrid combination of MC and MCF methods. The asterisks correspond to the free-diffusion signals. The two curves for each b-value are barely distinguishable.

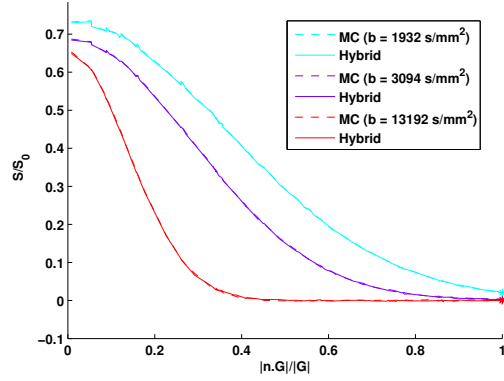


Figure 4: **Hybrid method yields ground-truth results for Gamma-distributed cylinders.** Total signal of so-called Gamma-distributed cylinders obtained by complete MC simulations (dashed curves, considered exact) and our hybrid approach (solid curves). The asterisks correspond to the free-diffusion signals. The two methods are again almost perfectly identical.

Defining the precision p as the inverse of the standard deviation, we obtain the precision p_H associated with the hybrid signal

$$p_H = \frac{\sqrt{N_H}}{f_{ex} \sigma_W}, \quad (8)$$

while the precision p_M of a complete MC simulation performed with a total of N_M spins can be written as

$$p_M = \frac{\sqrt{N_M}}{\sigma_W}, \quad (9)$$

assuming intra-axonal and extra-axonal spin phases are identically distributed.

We can now analyze the gain in precision-efficiency trade-off through three different situations, illustrated in Figure 6.

- **Fixed diffusion environment.** For a given intra-axonal volume fraction f_{in} where the MCF method is applicable, we predict the simulation times t_H and t_M of the two methods as a function of the desired

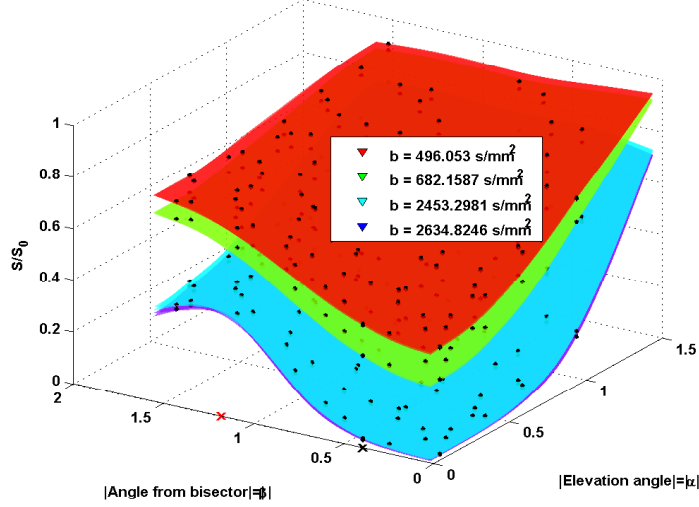


Figure 5: **Hybrid method yields ground-truth results for crossing cylinders.** Signal of fascicles crossing at an angle $\theta = \pi/4 \approx 0.785$ rad, obtained by complete MC simulations, considered exact, and our hybrid approach. The surfaces are obtained by smooth interpolation of the actual data points, in black (90 points per shell per method). The MC and hybrid surfaces are almost indistinguishable, except near $\beta \approx 1.5$ rad. The black marker at $(\alpha, \beta) = (0, \frac{\theta}{2})$ corresponds to the presence of fascicles either side of the bisector while the red marker at $(\alpha, \beta) = (0, \frac{\pi}{2} - \frac{\theta}{2})$ indicates the direction perpendicular to either fascicle in the fibers' plane ($\alpha = 0$), where a signal maximum seems to occur.

precision p as

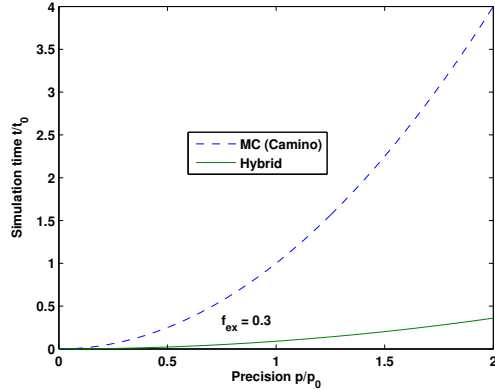
$$\begin{aligned} t_H &= t_0 N_H = t_0 \sigma_W^2 f_{ex}^2 p^2 \\ t_M &= t_0 N_M = t_0 \sigma_W^2 p^2, \end{aligned} \quad (10)$$

where the common factor t_0 accounts for the number of time steps and of PGSE sequences. There is therefore a gain factor f_{ex}^2 for the hybrid method, which is non-negligible for typical values $f_{ex} \approx 0.3$, leading to a reduction of 81% in computation time for the same precision, as shown in Figure 6a.

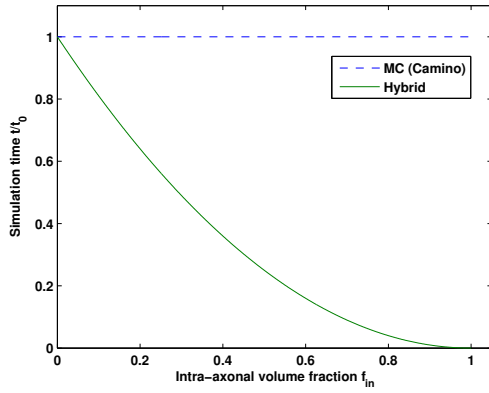
- **Fixed precision.** Figure 6b illustrates Eq. (10) as a function of the intra-axonal volume fraction f_{in} , for a given precision. We see the advantage of using the hybrid method, especially for typical microstructural values $f_{in} \geq 0.5$.
- **Fixed simulation time.** If we set $N_H = N_M = N$, then the precision p_M of a MC simulation will remain constant irrespective of the intra-axonal volume fraction f_{in} , i.e. $p_M = \frac{\sqrt{N}}{\sigma_W}$, while the precision p_H of the hybrid method evolves as

$$p_H = \frac{\sqrt{N}}{\sigma_W (1 - f_{in})}, \quad (11)$$

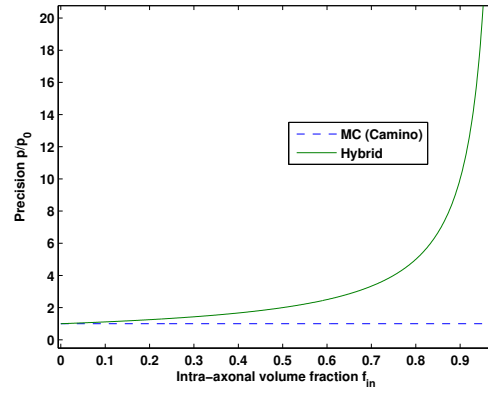
tending to the (nearly) infinite precision of the MCF approach when there is no extra-axonal space, as presented in Figure 6c.



(a) Simulation time vs precision



(b) Simulation time vs intra-axonal volume fraction



(c) Precision vs intra-axonal volume fraction

Figure 6: **Hybrid method leads to gain in precision-efficiency trade-off for commonly-used microstructural configurations.** The reference values t_0 and p_0 include factors common to both methods, such as the number of PGSE sequences or the number of time steps used. These results hold when part of the signal arises from geometric compartments where the MCF method is applicable.

4. CONCLUSION

Various configurations of the cerebral tissue microstructure can be adequately represented as an arrangement of cylindrical and spherical compartments. Given the availability of closed form formulas for the diffusion signal arising from such simple compartments, computationally-intensive MC simulations are not required for the simulation of signal arising from water molecules inside these compartments. Conversely, no analytical expression can accurately represent the diffusion signal arising from extracellular water molecules whose diffusion is hindered by tissue barriers. For those water molecules, MC simulation is a reliable approach to predict the diffusion-weighted MRI signal. This paper introduced a hybrid method for the simulation of diffusion-weighted MRI signal arising from both intra-cellular and extra-cellular water molecules by taking advantage of analytical solutions for intra-cellular compartments and MC simulation for extra-cellular compartments. This approach leads to an important decrease in simulation time for an identical desired precision, especially as the extra-cellular volume fraction decreases. For typically-encountered intra-axonal volume fractions of about 0.7, less than a fifth of the simulation time is necessary. Conversely, the presented method leads to superior precision levels for a given simulation time. This novel hybrid approach can therefore be used for simulations of diffusion-weighted MRI signals in a large number of microstructural configurations.

REFERENCES

- [1] Alexander, D. C. and Barker, G. J., “Optimal imaging parameters for fiber-orientation estimation in diffusion mri,” *Neuroimage* **27**(2), 357–367 (2005).
- [2] Auría, A., Daducci, A., Thiran, J.-P., and Wiaux, Y., “Structured sparsity for spatially coherent fibre orientation estimation in diffusion MRI,” *NeuroImage* (2015).
- [3] Scherrer, B. and Warfield, S. K., “Parametric representation of multiple white matter fascicles from cube and sphere diffusion MRI,” *PLoS one* **7**(11), e48232 (2012).
- [4] Zhang, H., Schneider, T., Wheeler-Kingshott, C. A., and Alexander, D. C., “NODDI: practical in vivo neurite orientation dispersion and density imaging of the human brain,” *Neuroimage* **61**(4), 1000–1016 (2012).
- [5] Assaf, Y., Freidlin, R. Z., Rohde, G. K., and Basser, P. J., “New modeling and experimental framework to characterize hindered and restricted water diffusion in brain white matter,” *Magnetic Resonance in Medicine* **52**(5), 965–978 (2004).
- [6] Scherrer, B., Schwartzman, A., Taquet, M., Prabhu, S. P., Sahin, M., Akhondi-Asl, A., and Warfield, S. K., “Characterizing the distribution of anisotropic micro-structural environments with diffusion-weighted imaging (DIAMOND),” in [*Medical Image Computing and Computer-Assisted Intervention–MICCAI 2013*], 518–526, Springer (2013).
- [7] Grebenkov, D. S., “NMR survey of reflected brownian motion,” *Reviews of Modern Physics* **79**(3), 1077 (2007).
- [8] Alexander, D. C., Hubbard, P. L., Hall, M. G., Moore, E. A., Ptito, M., Parker, G. J., and Dyrby, T. B., “Orientationally invariant indices of axon diameter and density from diffusion MRI,” *Neuroimage* **52**(4), 1374–1389 (2010).
- [9] Fieremans, E., Novikov, D. S., Jensen, J. H., and Helpert, J. A., “Monte carlo study of a two-compartment exchange model of diffusion,” *NMR in Biomedicine* **23**(7), 711–724 (2010).
- [10] Price, W. S., [*NMR studies of translational motion: principles and applications*], Cambridge University Press (2009).
- [11] Assaf, Y., Blumenfeld-Katzir, T., Yovel, Y., and Basser, P. J., “Axciliber: a method for measuring axon diameter distribution from diffusion MRI,” *Magnetic Resonance in Medicine* **59**(6), 1347–1354 (2008).
- [12] Brezis, H., [*Functional analysis, Sobolev spaces and partial differential equations*], Springer Science & Business Media (2010).
- [13] Cook, P., Bai, Y., Nedjati-Gilani, S., Seunarine, K., Hall, M., Parker, G., and Alexander, D., “Camino: open-source diffusion-MRI reconstruction and processing,” in [*14th scientific meeting of the international society for magnetic resonance in medicine*], **2759** (2006).
- [14] Hall, M. G. and Alexander, D. C., “Convergence and parameter choice for Monte-Carlo simulations of diffusion MRI,” *Medical Imaging, IEEE Transactions on* **28**(9), 1354–1364 (2009).
- [15] Tuch, D. S., Reese, T. G., Wiegell, M. R., Makris, N., Belliveau, J. W., and Wedeen, V. J., “High angular resolution diffusion imaging reveals intravoxel white matter fiber heterogeneity,” *Magnetic Resonance in Medicine* **48**(4), 577–582 (2002).